L’integrazione di tecniche fotogrammetriche e MMS nel rilievo metrico dei Beni Culturali

A preliminary CFD and tritium transport analysis for ARC blanket

Gabriele Ferrero, Samuele Meschini, Raffaella Testoni*

Dipartimento Energia "Galileo Ferraris", Politecnico di Torino, Corso Duca degli Abruzzi, 24 – Torino (Italy)

* Corresponding author: raffaella.testoni@polito.it

Telephone number: +39 0110904494

A preliminary CFD and tritium transport analysis for ARC blanket

Gabriele Ferrero, Samuele Meschini, Raffaella Testoni*

Dipartimento Energia "Galileo Ferraris", Politecnico di Torino, Corso Duca degli Abruzzi, 24 – Torino (Italy)

* Corresponding author: raffaella.testoni@polito.it

Abstract

ARC (Affordable, Robust, Compact) fusion reactor is a preconceptual design proposed by the Plasma Science and Fusion Center at the Massachusetts Institute of Technology which will be developed by Commonwealth Fusion Systems. ARC features a Li_2BeF_4 (FLiBe) molten salt liquid blanket that provides reactor cooling, neutron shielding, and tritium breeding. This work aims to develop a preliminary coupled CFD and tritium transport model to describe FLiBe flow inside the tank and to assess ARC tritium inventory in the vacuum vessel and blanket. Both models are built by taking advantage of COMSOL® Multiphysics. FLiBe velocity and temperature fields are evaluated by the CFD models, and they are passed as input to the tritium transport model. The tritium transport model computes tritium concentration inside solid materials and FLiBe. An auxiliary FLiBe inlet has been moved from the original position in the ARC pre-conceptual design to improve blanket cooling and to reduce the size of flow eddies. Results show that many recirculation zones generate inside the tank for the chosen tank geometry, size, and inlet-outlet conditions. Larger FLiBe temperature and tritium concentration are found in these zones. The high FLiBe temperature in recirculation areas may not allow for effective cooling, and Inconel 718 reaches critical temperatures. The largest tritium concentration for a steady-state model with continuity of tritium partial pressure at the interfaces is found in Inconel 718, while the second-highest concentration is reached in FLiBe. The total tritium inventory in ARC blanket with the assumed model is quantified as 3.16 g.

Keywords: ARC, Tokamak, Blanket, CFD, Tritium transport.

I. Introduction

ARC reactor (Affordable, Robust, and Compact) is a fusion reactor project designed by the Massachusetts Institute of Technology and Plasma Science and Fusion Center[1] and under development at Commonwealth Fusion Systems. ARC is conceived to be smaller than other fusion power plants, but with higher power density. The goal is to reduce size and complexity to make the reactor cheaper. ARC exploits the newest technologies available, such as high temperature superconducting magnets and an innovative liquid breeding blanket design to achieve this goal. A preliminary conceptual design of ARC was proposed by Sorbom et al. [1]. More recent studies investigated ARC power exhaust[2], the divertor design [3] and tritium inventory at system level [4][5]. This paper focuses on the Li_2BeF_4 molten salt (FLiBe) breeding blanket. A CFD and tritium transport analysis is carried out. A mesh convergence study is provided as well to assess the accuracy of the results. This preliminary study is an important step to evaluate how FLiBe could behave inside the blanket and to estimate blanket tritium inventory, which is crucial for ARC economy, design, and safety. This analysis allows to make important geometry considerations on current ARC pre-conceptual design and to investigate if criticalities arise to address them in further design evolutions.

II. Methodological approach

The objective of this work is a preliminary analysis of tritium transport and distribution inside the blanket of the reactor. The study starts from a CFD model applied to the blanket to evaluate temperature, velocity, and pressure fields that characterize the molten salt dynamics in the reactor blanket. MHD phenomena are not considered for this analysis. As a matter of fact, the impact of MHD on the system is estimated to be lower for molten salts than in liquid metal systems [2], due to lower electrical conductivity. A detailed MHD analysis will still be needed due to the high magnetic fields employed in ARC, which are estimated to be above 9.2 T [1]. MHD phenomena should impact

heat transfer coefficient, due to turbulence suppression diminishing Nusselt number up to 30%[6]. For the heat/mass transfer analogy, Sherwood number is expected to diminish as well.

Figure 1 shows a flowchart that depicts the main steps of the analysis.

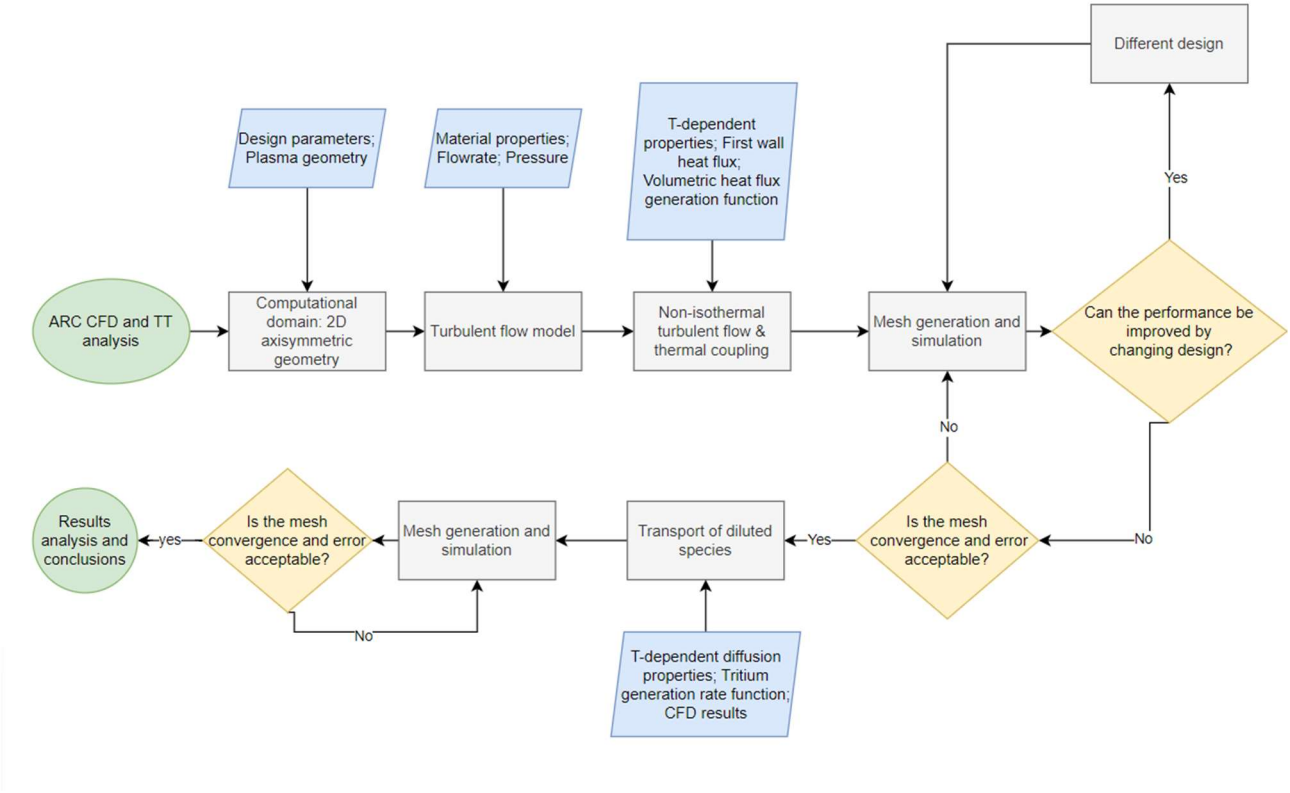

Figure 1 Flowchart for the CFD and tritium transport. TT stands for Tritium Transport.

For FLiBe fluid domain, Navier-Stokes equations[7] for momentum and mass conservation are employed, including buoyancy phenomena. Conduction-convection heat transfer equation is applied to each ARC wall layer and to the FLiBe breeding blanket. Heat flux applied on the first wall is approximated as uniform, while the heat generation rate in the breeding blanket follows an exponential profile. Navier-Stokes and heat equations have been coupled to determine velocity and temperature fields. Realizable k-Ɛ model has been chosen because of its better performance with recirculating flows [8] with respect to the classic k-Ɛ model [9][10].

Temperature and pressure fields from the CFD analysis are used as input for the tritium transport model, which is exploited to evaluate tritium inventories in FLiBe and structural materials for steady state-conditions and a reactor power of 658 MW adapted from [11].

In this respect, this work focuses mainly on tritium present in the FLiBe fluid as well as in the main structures in T_2 form. Indeed, , tritium in FLiBe is expected to be present primarily in the form of T_2 in the strongly-reducing conditions needed for corrosion control [12]. Moreover, tritium as TF, which is the specie in which tritium is generated, would not diffuse through solid structures. While TF concentration investigations are needed to evaluate corrosion impact on the system, these would need different modeling and are outside the scope of the paper. Tritium transport in ARC is evaluated starting from the general transport equation in a diffusion-limited steady-state model (DLM), which neglects surface effects. This approximation can be done if the dimensionless number [13]:

$$W' = \frac{k_d x \sqrt{p}}{D K_s} \gg 1$$

where k_d is the dissociation constant $[mol/m^2 \cdot s \cdot Pa]$, x is material thickness $[m]$, p is tritium partial pressure $[Pa]$, D is the tritium diffusion coefficient $[m^2/s]$ and K_S is Sievert constant $\left[{mol}/{m^3\ Pa^{1/2}}\right]$ for the materials involved. At 900 K, $W'_{Inc} = 610$ and $W'_{Be} = 25219$, hence W'>>1 is satisfied for each ARC material in contact with FLiBe. However, it is difficult to measure k_d and there is no value in literature for Inconel 718 and beryllium, therefore some values have been assumed equal to other similar materials (Inconel 625) available in literature $k_{d,Inc625} = 5.2 \cdot 10^{-5} e^{\frac{33}{RT}}\ [mol/m^2 \cdot s \cdot Pa]$, being T in $[K]$ and the activation energy in $[kJ/mol]$ [14]. If parameters are not known, DLM transport is assumed [15]. FOR DLM transport s driven only by Fick's law:

$$\frac{\delta c_i}{\delta t} + \nabla \cdot \vec{u} c_i - \nabla \cdot (D_i \nabla c_i) = s \qquad (1)$$

where c_i $[mol/m^3]$ is the tritium concentration in the i-th material domain (Tungsten, Inconel 718, Beryllium, FLiBe), $\vec{u}$ $[m/s]$ is the velocity vector, D_i $[m^2/s]$ is tritium diffusion coefficient in the i-th material and s $[mol/m^3/s]$ is the tritium generation source. In steady-state conditions, $\frac{\delta c}{\delta t} = 0$. Tritium generation is assumed negligible in materials different from FLiBe. Inlet concentration c_{in} $[mol/m^3]$ for FLiBe dependents on outlet concentration c_{out} and tritium extraction system efficiency η_{TES}:

$$c_{in} = c_{out}\,(1 - \eta_{TES}) \tag{2}$$

Tritium concentration in FLiBe is driven by inlet conditions, tritium volumetric generation, tritium diffusion, and advection. Tritium concentration outside the FLiBe domain is evaluated by a DLM with an imposed partial pressure at the interface of each domain. For molten salt domains such as FLiBe, the partial pressure of the solute atoms in steady-state is evaluated by Henry's Law:

$$c_i = k_H p_i \tag{3}$$

where c_i is T_2 concentration, k_H $\left[{mol}/{m^3\ Pa}\right]$ is Henry's constant and p_i $[Pa]$ is tritium partial pressure. For metal membranes, the equilibrium concentration of the solute atoms in steady-state is evaluated by Sieverts' Law:

$$c_i = k_S\sqrt{p_i} \tag{4}$$

where the Sieverts' constant $k_S = \sqrt{\frac{K_d}{K_r}}$ $\left[{mol}/{m^3\ Pa^{1/2}}\right]$ derives from the equilibrium of dissociative adsorption (K_d) and recombinative desorption phenomena (K_r) and p_i $[Pa]$ is tritium partial pressure. Tritium concentration in solid domains is evaluated with the assumption of partial pressure continuity, by setting a partition condition on each domain interface.

$$\frac{c_r}{c_l} = K \tag{5}$$

where c_r and c_l are the concentrations on the opposite sides of the boundary and K is the partition coefficient. $K = \frac{k_{S,r}}{k_{S,l}}$ for metal-metal boundaries and $K = \frac{c_m \cdot k_H}{k_S{}^2}$ for metal-liquid boundaries have been set to preserve partial pressure continuity, where c_m is the concentration in the metal domain itself. External layer boundary conditions are assumed as adiabatic (no flux) as a conservative guess, leading to maximum tritium inventory.

A mesh convergence study has been carried out for both the CFD and tritium transport models according to the reference procedure described by Roache et al.[16], using the Richardson extrapolation [17] as suggested by the ERCOFTAC Best Practice Guidelines for Industrial Applications[18]. This method can estimate the order of accuracy of the results "a posteriori" from the results of three different hybrid meshes: M1 (finer), M2 (reference mesh) and M3 (coarser). The Grid Convergence Index (GCI) is the reference parameter to assess the mesh accuracy.

III. Geometry and input data

III.A ARC geometry and computational domain

ARC reactor preconceptual design foresees a double wall Vacuum Vessel (VV) immersed into a bulk FLiBe tank. The design [1] includes a 1 mm thick Tungsten first wall supported by a 10 mm Inconel 718 layer, a 20 mm thick FLiBe channel between the two vacuum vessel walls and the second wall composed of a 10 mm thick Beryllium layer and a 30 mm thick Inconel 718 layer (Figure 2). ARC breeding blanket is the FLiBe flowing both inside the vacuum vessel channel and the tank the vacuum vessel is immersed in. In this particular design, the liquid breeding blanket, which is composed of the flowing FLiBe, absolves the role of coolant, tritium breeder, tritium carrier, and neutronic shield. For the 2D axisymmetric model, a connection between the vacuum vessel channel and the tank has been hypothesized (Figure 2).

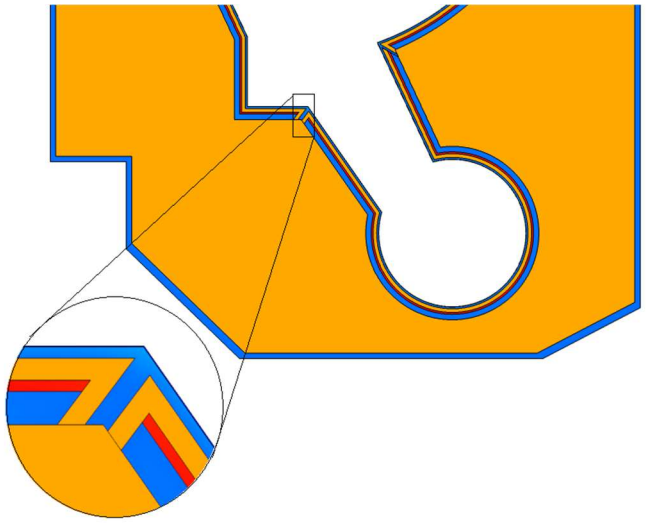

Figure 2 ARC vacuum vessel geometry, different colors are used for different materials. (Orange: FLiBe; Blue: Inconel; Red: Beryllium; Tungsten layer is too thin to be seen).

ARC geometry was built with COMSOL® CAD tools, starting from known design parameters [1], available mainly for the external tank, and adapting unknown measures for the vacuum vessel with ARC plasma shape ($\text{elongation} = 1.8, \text{triangularity} = 0.375, \text{ minor radius} = 1.13$ m). Geometry is 2D axisymmetric (Figure 3). Vacuum vessel and tank are both included in the same geometry model and in the same study to precisely simulate convective heat transfer between the two components, as local hotspots in the tank can greatly influence vacuum vessel temperature.

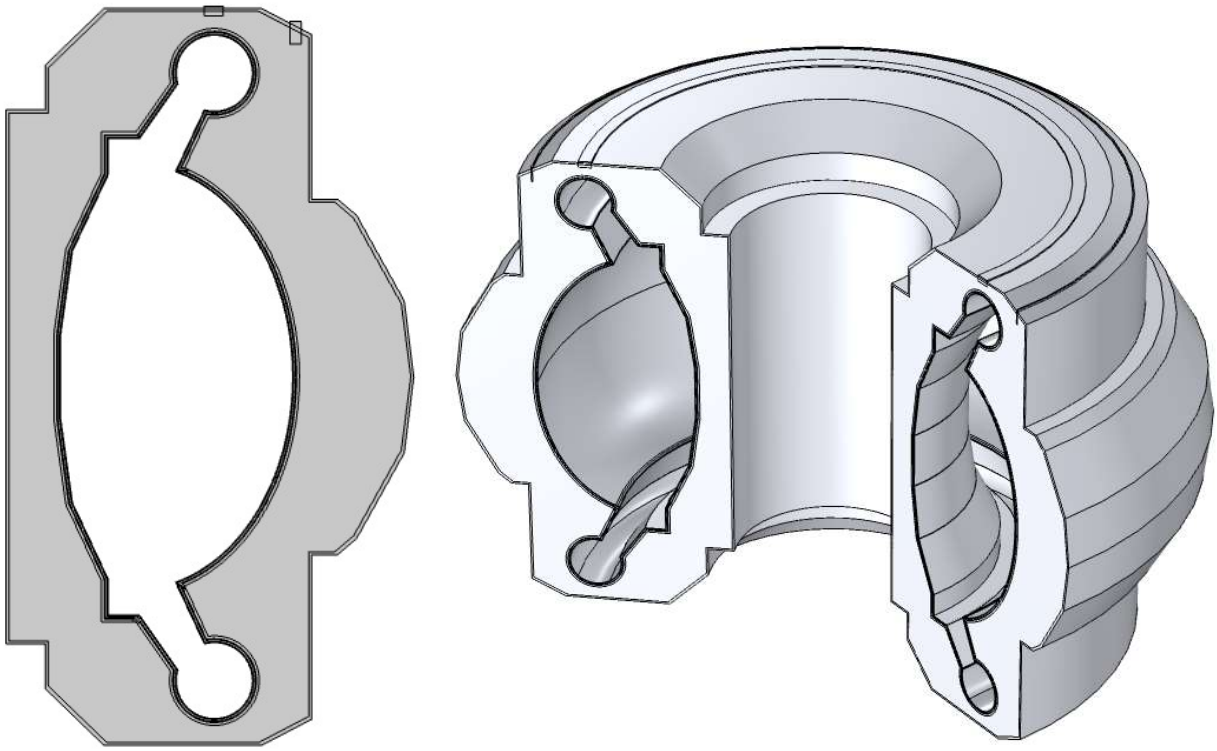

Figure 3 2D axisymmetric computational domain of ARC and its revolution geometry

Initial ARC geometry is adapted to simulate inlets and outlets configuration proposed by Kuang et al. [2] by connecting the vacuum vessel channels with the external tank (Figure 2), moving tank auxiliary inlet from the suggested location (Figure 4). Inlets for the vacuum vessel channel are located

ideally in the vacuum vessel channel itself, while more mature design stages will include more realistic connections and inlets.

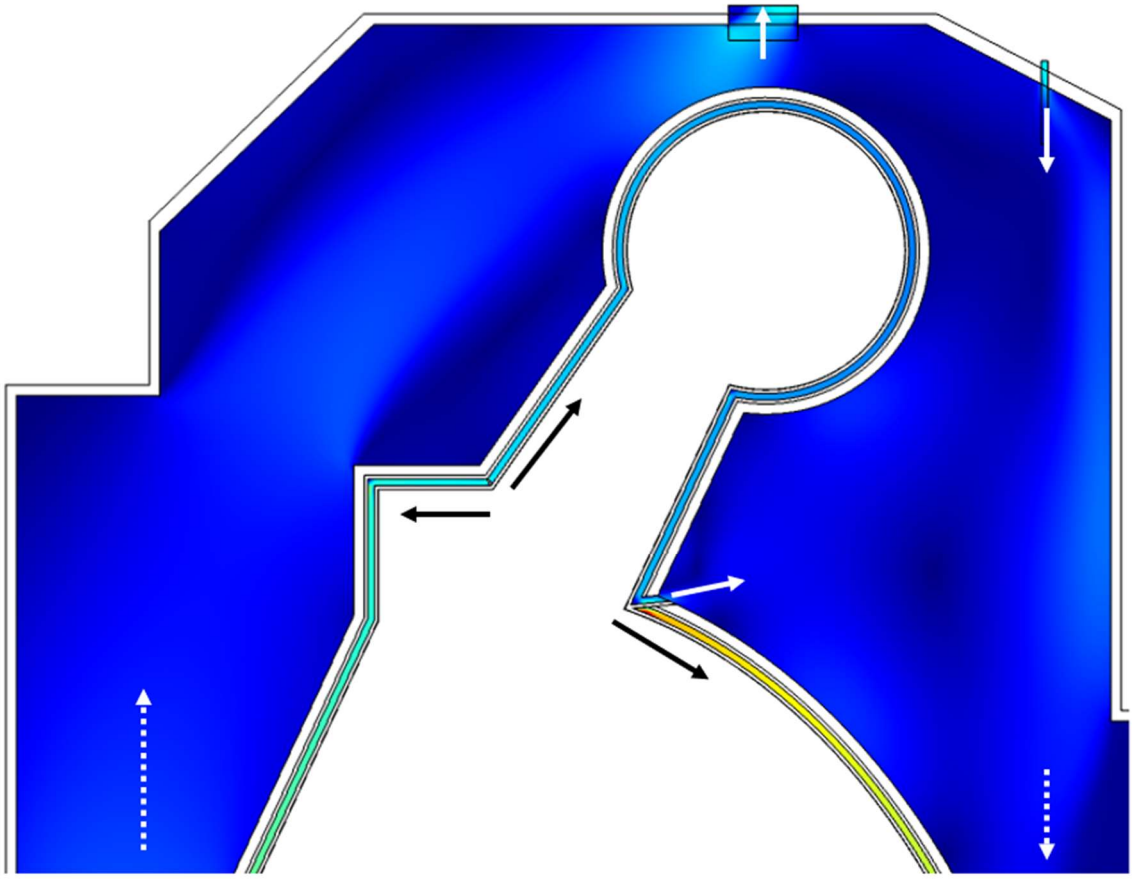

Figure 4 Inlet-outlet configuration in ARC vessel and tank. The auxiliary inlet has been moved from the initial configuration defined in [2].

III.B CFD model

First, the CFD analysis was carried out. Inlet condition vary for each inlet and are chosen to conserve the mass flow rate needed to obtain a temperature jump of 100 K measured at the outlet . A velocity threshold for corrosion issues has been considered at 2 m/s [1] as an educated guess as there is little data on flow-aided corrosion for FLiBe. It is reasonable to think that corrosion phenomena will be exacerbated by high temperatures and high flow rates [2]. From preliminary evaluations [19], it seems that it will be necessary due to selective Cr corrosion. After an in-depth analysis, the need for a corrosion control system for ARC will become clearer. Inlet boundary conditions are set to fully

developed flow. Turbulent flow condition is set in the channel region and in the tank region. Pressure at the outlet is set equal to $3\ bar$. A constant plasma heat flux of $0.5\ MW/m^2$ is applied to the first wall [2]. This is an approximation made necessary by the insufficient data on ARC first wall heat flux distribution available in literature. Also, such type of evaluation is outside of the scope of the work and would need a different analysis. Clearly, there are some regions that are expected to experience much higher thermal loads (i.e. divertors). However, they will have a dedicated and optimized coolant system [2]. For sake of simplicity, thermal flux in these regions has been set equal to the rest of the vessel chamber wall. Volumetric heat generation rates, evaluated from neutronic simulations [11], are assumed constant for each vacuum vessel layer (TABLE I), while they follow a decreasing exponential profile from the vacuum vessel external surface throughout the tank region. The exponential fit for volumetric power generation in the bulk FLiBe is then:

$$\dot{q} = 5.0776e^{-8.209x}\left[{MW}/{m^3}\right] \tag{6}$$

Tank and vacuum vessel regions are included in the same model to evaluate convection between the two regions without approximations. FLiBe temperatures for channel and tank inlets are set at $800\ K$. Material properties are temperature-dependent (TABLE II).

TABLE I Volumetric power distribution in ARC adapted from [11].

Domain	**Volumetric power generation MW/m^3**
Tungsten	21.7
Inconel 718 (inner)	10.1
FLiBe channel	9.64
Beryllium	5.58
Inconel 718 (outer)	6.56
FLiBe tank average	0.8
Inconel 718 (shell)	0.04

TABLE II Material properties as a function of temperature

	Inconel 718 [21]
$k\ [W/(m \cdot K)]$	$3.495867 + 2.673305 \cdot 10^{-2} \times \mathrm{T} - 1.11803 \cdot 10^{-5} \times T^2 + 3.606836 \cdot 10^{-9} \times T^3 + 8.235547 \cdot 10^{-14} \times T^4$
$\rho\ [kg/m^3]$	8.19
$c_p\ [J/(kg \cdot K)]$	$361.3373 + 0.2378248 \times T + 7.560689 \cdot 10^{-6} \times T^2$
	Tungsten [20]
$k\ [W/(m \cdot K)]$	$240.51 - 0.2899 \times T + 2.5403 \cdot 10^{-4} \times T^2 - 1.0263 \cdot 10^{-7} \times T^3 + 1.5238 \cdot 10^{-11} \times T^4$
$\rho\ [kg/m^3]$	$19302.7 - 2.3786 \cdot 10^{-1} \times T - 2.2448 \cdot 10^{-5} \times T^2$
$c_p\ [J/(kg \cdot K)]$	$116.37 + 7.1119 \cdot 10^{-2} \times T - 6.5828 \cdot 10^{-5} \times T^2 + 3.2396 \cdot 10^{-8} \times T^3 - 5.4523 \cdot 10^{-12} \times T^4$
	Beryllium [21] [22]
$k\ [W/(m \cdot K)]$	$430.35 - 1.1674 \times T + 1.6044 \cdot 10^{-3} \times T^2 - 1.0097 \cdot 10^{-6} \times T^3 + 2.3642 \cdot 10^{-10} \times T^4$
$\rho\ [kg/m^3]$	1848
$c_p\ [J/(kg \cdot K)]$	$606.91 + 5.3382 \times T - 4.1726 \cdot 10^{-3} \times T^2 + 1.2723 \cdot 10^{-6} \times T^3$
	FLiBe [23]
$k\ [W/(m \cdot K)]$	1.1
$\rho\ [kg/m^3]$	$2413.10646 - 0.4884 \times T$
$c_p\ [J/(kg \cdot K)]$	2386
$\mu\ [Pa \cdot S]$	$1.16 \cdot 10^{-4} \times e^{3755/T}$

Where $c_p = heat\ capacity$, $k = thermal\ conductivity$, $\rho = density$, $\mu = dynamic\ viscosity$.

III.C Tritium transport model

FLiBe temperature and flow fields from CFD are included as input in tritium transport model. COMSOL® *Transport of diluted species* is used for this simulation. Tritium diffusion coefficients and Sieverts' constant for Tungsten[20], Inconel 718[21], Beryllium [22] and Henry's constant for FLiBe [23] are listed in TABLE III. Transport properties, such as Henry's constant, Sieverts' constants, and diffusion coefficients follow a temperature dependence law in the form of an Arrhenius equation. Tritium generation in the FLiBe follows an exponential profile evaluated through neutronic simulations in previous works [11]. The exponential fit for tritium generation data is:

$$\dot{T} = 5.00 \cdot 10^{-6} e^{-8.41x} [\, mol/s \cdot m^3] \qquad (7)$$

Tritium concentration inlet condition for channel and tank is set by Eq. (2), with $\eta_{TES} = 0.8$, which is a reference value of a theoretically achievable extraction efficiency employing Permeation Against Vacuum or Vacuum Sieve Tray systems [24].

TABLE III Transport properties (Sieverts' and Henry's constant) for ARC materials at each material operating temperature.

Domain	Value	Diffusion coefficient $[m^2/s]$
FLiBe	$k_{h.FLiBe} = 4.54 \cdot 10^{-4}\, mol/m^3 \cdot Pa$	$9.3 \cdot 10^{-7} exp\left(\frac{-43E3\ {}^{J}/_{mol}}{R \cdot T}\right)$
Tungsten	$k_{S,W} = 1.5 \cdot 10^{-4}\ mol/m^3 Pa^{1/2}$	$4.1 \cdot 10^{-7} exp\left(\frac{-4.527}{T}\right)$
Beryllium	$k_{S,Be} = 0.0015\ mol/m^3 Pa^{1/2}$	$48 \cdot 10^{-9} exp\left(\frac{-3.5E4\ {}^{J}/_{mol}}{R \cdot T}\right)$
Inconel 718	$k_{S,Inc} = 0.058\, mol/m^3 Pa^{1/2}$	$10^{\left(-5.98-\left(\frac{0.52\ {}^{eV}/_{mol}}{2.303 \cdot R \cdot T}\right)\right)}$

IV. Results

In this section, the main results obtained with the previously explained models and methods are presented. First, the accuracy of CFD and tritium transport results is shown in terms of mesh convergence (Section IV.A). The CFD results are described in Section IV.B. Section IV.C reports on tritium inventories inside the reactor taking into account the previous CFD results.

IV.A Mesh convergence

Mesh convergence and grid convergence indexes (GCI) were evaluated for both CFD and tritium transport studies. As far as the CFD analysis is concerned, Figure 5 shows the estimated GCI for the selected parameters of the CFD study. All the parameters show a GCI lower than 2%. For the most refined mesh GCI is below 1%. Tritium transport analysis shows a GCI below 5% for all the

parameters except for Inconel shell layer concentration, where a GCI of 6.35 % has been found. For the purpose of this work, the degree of uncertainty is considered acceptable. In Figure 6, a detail of the mesh used for the analysis is reported, specifying the different domains.

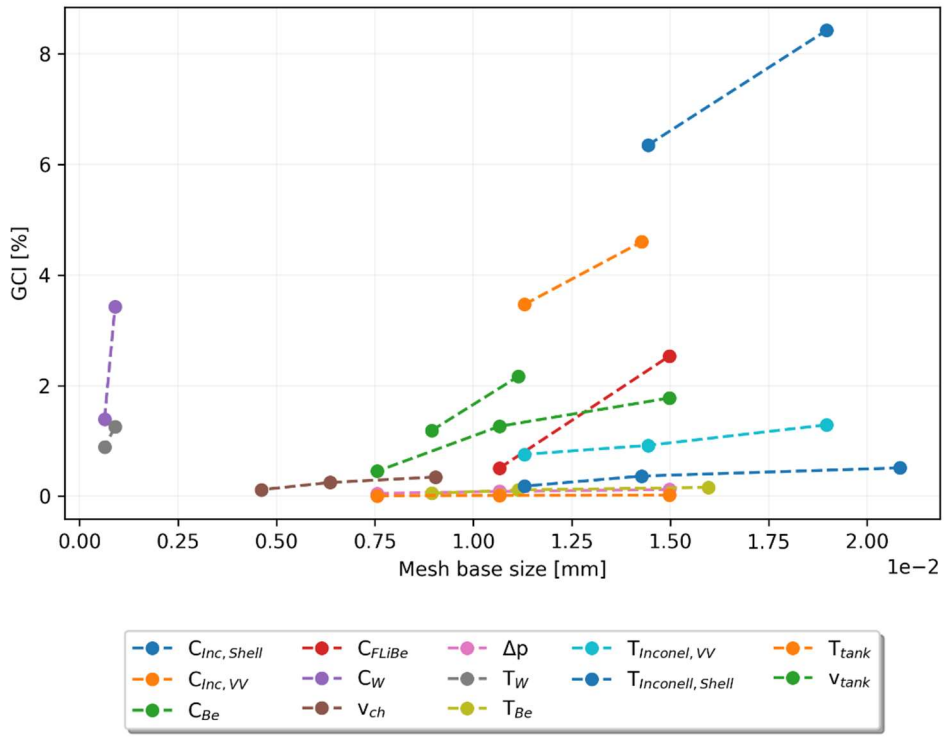

Figure 5 GCI for CFD and transport results as a function of mesh size

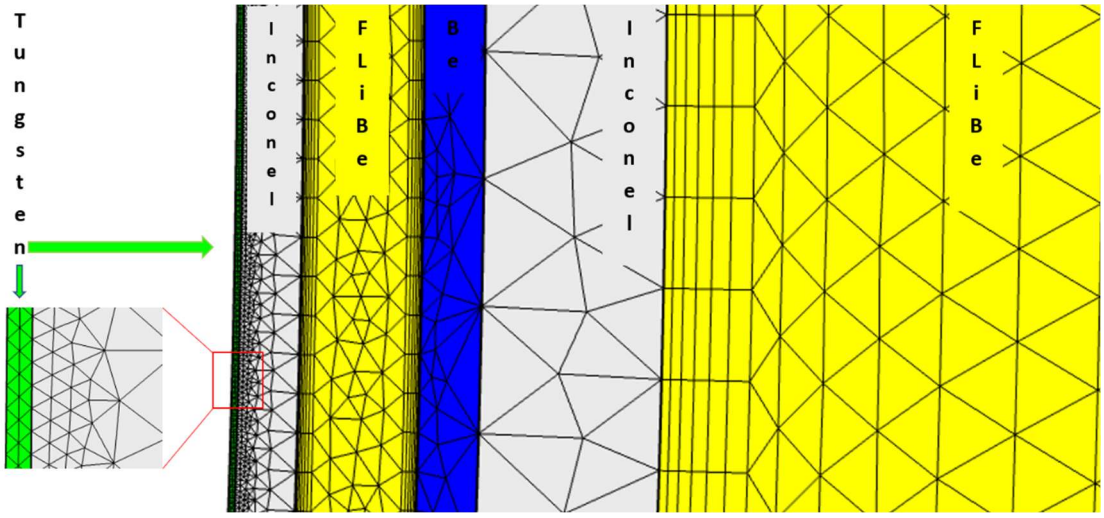

Figure 6 Mesh used for the simulations.

IV.B CFD analysis

IV.B.1 Channel CFD analysis

Velocity and temperature fields for vacuum vessel channels are reported in this section. As the objective of this study is a preliminary evaluation of tritium concentration across the reactor, a simplified design of the vacuum vessel channel has been considered to reduce the computational domain to 2D. FLiBe velocity through vacuum vessel channels depends on the distance from the toroidal symmetry axis, as the channel section gets smaller towards the symmetry axis, making FLiBe flow faster. While the 2D axisymmetric model cannot represent a realistic engineering design and leads to a significantly different geometry, considerations like FLiBe acceleration flowing towards the toroidal axis are still valid and should be accounted in the design phase. For this reason, it is observed that the vacuum vessel division in different sections proposed by Kuang et al. [2]is beneficial to uniform the flow field. Indeed, FLiBe experiences a lower acceleration thanks to the lower Δr of channel segments, where Δr is the difference between the maximum and the minimum radial distance of the channel profile from the toroidal axis.

Due to the nature of the 2D model, inlet cross-sections are enlarged and have an annular shape. To conserve the system flow rate and temperature variations in the blanket, inlet velocities in the channels have been lowered as a consequence. However, further considerations on local accelerations and heat transfer coefficient in the channel have been made with different inlet conditions (2 m/s), which reflects better the velocity field in channel regions in a 3D design, where FLiBe will flow inside pipes. Each vacuum vessel section is different due to the geometrical layout, and may require different operational conditions and flowrates For the 2 m/s inlet conditions, the velocity at turning points such as the lower divertor channel outlet is highly affected by the vena contracta effect (Figure 7), making it a potential critical point for vessel corrosion.

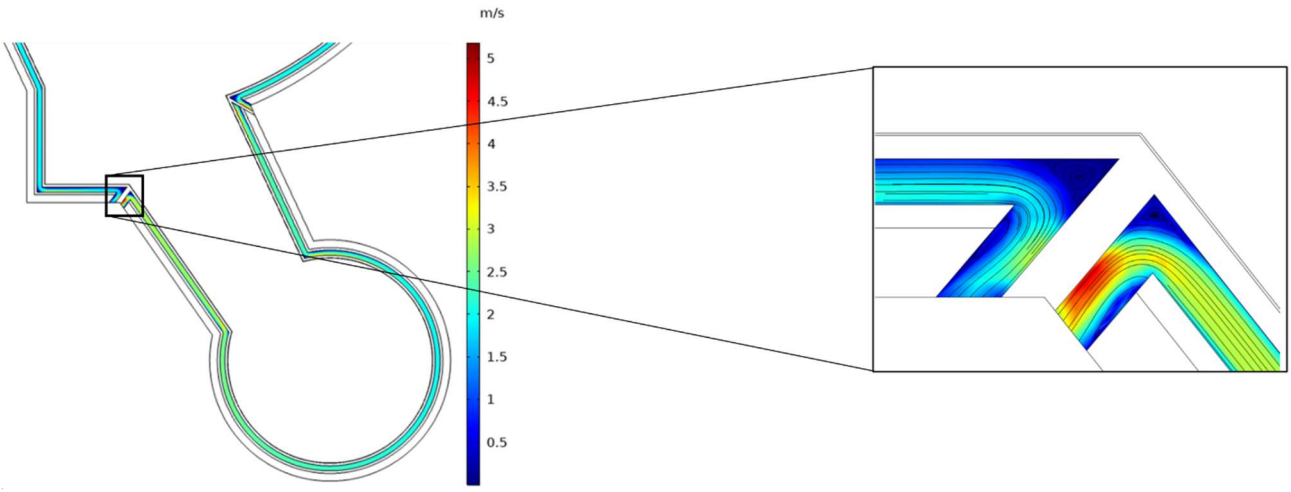

Figure 7 Vena contracta region due to sharp turnover in vessel channel.

The channel heat transfer coefficient has been evaluated with independent simulations by applying a constant heat flux on each wall singularly. Volumetric power generation inside FLiBe has been set to zero in these simulations. For this evaluation, a k-ω model with automatic wall functions has been employed in the outboard region channel. To ensure that adequate wall discretization was accomplished, the resolution of wall boundary layers was checked by the dimensionless wall distance evaluated at the first mesh cell next to the wall $\frac{h_w u_\tau}{\nu} < 1$, where $h_w$is the thickness of the first boundary layer cell u_τ is the friction velocity and ν is the kinematic viscosity. Heat transfer coefficient has been evaluated as $h = \frac{q}{\Delta T}$, being ΔT the difference between the channel wall temperature where the heat flux has been applied and FLiBe bulk temperature at the same height, and then h has been compared with Gnielinski correlation with good agreement. For the analyzed model, $h_{Be} \approx 1100\, W/(m^2 \cdot K)$ as average for the channel-beryllium wall, and $h_{Inc} \approx 1070\, W/(m^2 \cdot K)$ as average for the channel-Inconel wall, which are lower than previuos estimates[2]. This is expected because of the different channel geometry in the model and lower velocities involved. The heat transfer coefficients evaluated in the channel for the higher velocity inlet condition of $2m/s$ ($h_{Be,v=2m/s} = 10.1\ kW/(m^2 \cdot K)$; $h_{Inc,v=2m/s} = 10.2\, kW/(m^2 \cdot K)$) are still lower than previous estimates. Because of insufficient cooling, the Inconel 718 average temperature in the first layer (TABLE IV) is above the creep limit of 930 K[25]. A more complex

configuration which modifies fluidynamics conditions to enhance heat transfer with passive techniques, such as swirl tubes and wire coil inserts, will be considered and analyzed in further studies.

TABLE IV ARC average temperature for VV and blanket components.

Domain	Average Value
Inlet blanket	800 [K]
Mass Flow Rate	2757 $[kg/s]$
Outlet blanket	900 [K]
Tank	892 [K]
First Wall	1337 [K]
Inconel- First layer	1226 [K]
Beryllium	931 [K]
Inconel- Second Layer	979.5 [K]

IV.B.2 Tank CFD analysis

The analysis of ARC blanket tank shows a major FLiBe flow cooling down vacuum vessel external layers. Starting from the auxiliary tank inlet, it flows towards the vacuum vessel lower divertor. Then, a fraction of the flows goes towards the outlet, while the remaining fraction recirculates in the tank. This recirculation contributes to increasing FLiBe temperature in the tank region. Flowrates from vacuum vessel channels, which accounts for roughly 80% of total mass flowrate, progressively join this stream. Secondary FLiBe flows appear near both vacuum vessel walls and external tank shell corners (Figure 8). These eddies are responsible for hotspots in high power generation areas, namely close to the vacuum vessel. The comparison between models with and without buoyancy showcased how buoyancy phenomena help to uniform the temperature, representing an obstacle to the generation of eddy-induced hotspots (Figure 9).

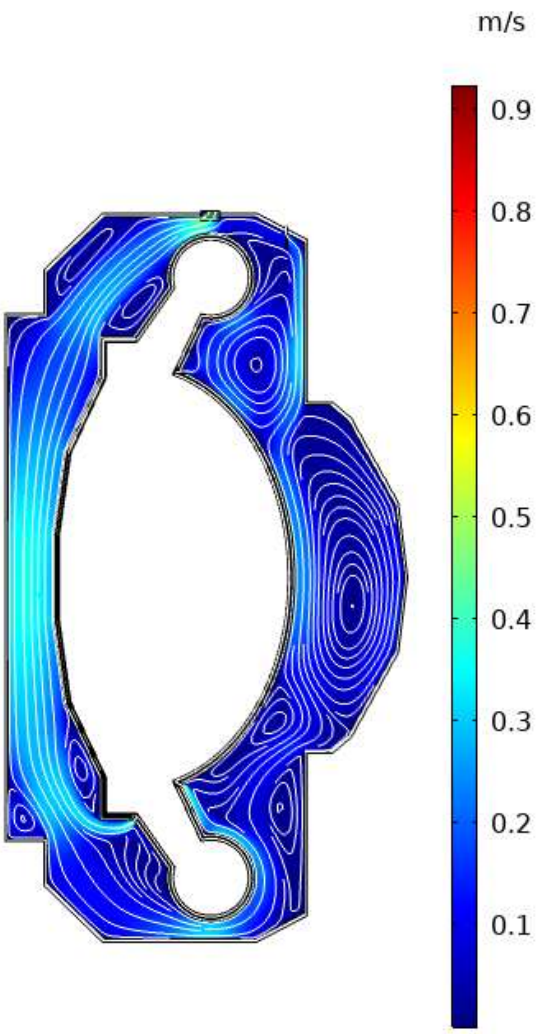

Figure 8 FLiBe velocity field and streamlines inside tank. Many eddies can be identified close to the VV walls and tank corners.

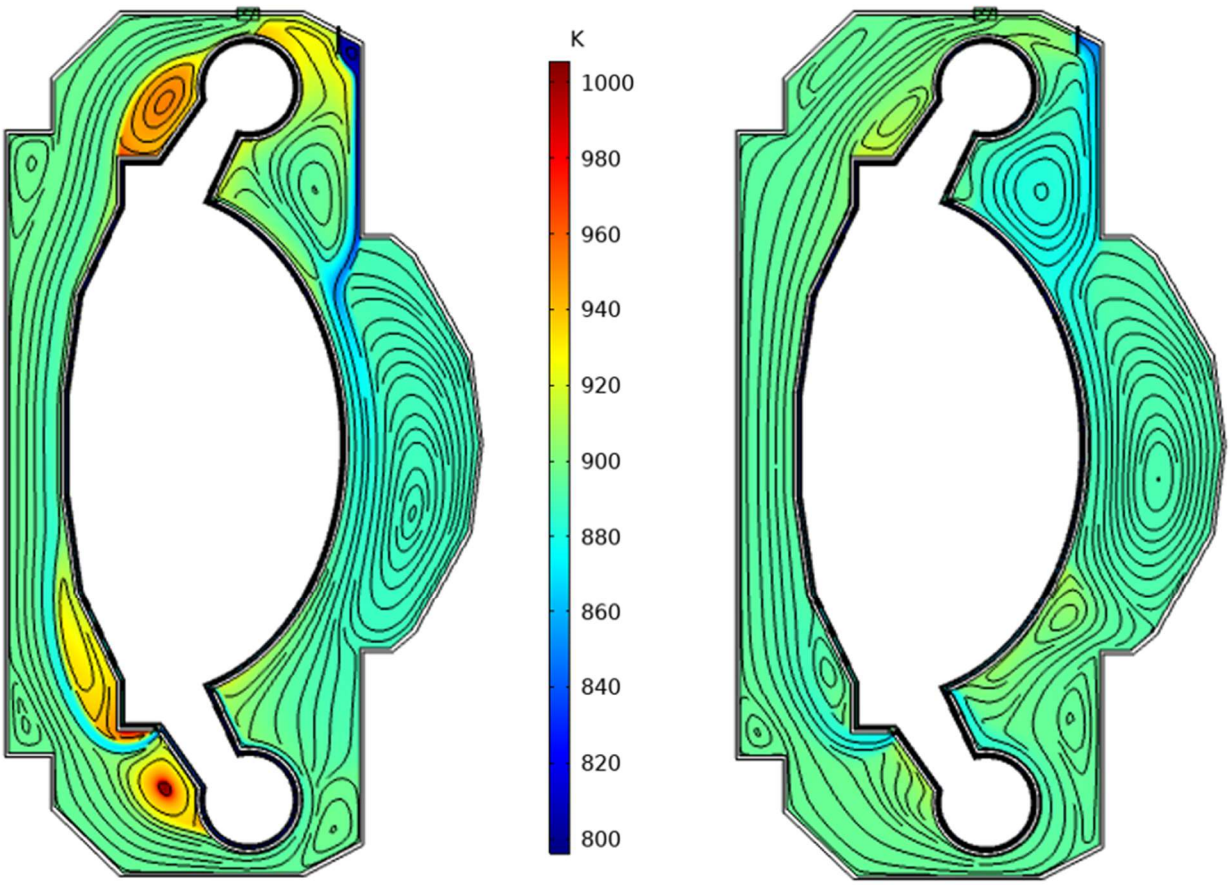

Figure 9: ARC Temperature distribution without buoyancy (left) and with buoyancy (right).

A critical area is found close to the inner vacuum vessel outlet near the lower divertor leg (Figure 10). The hotspot originates from recirculating flows of high-temperature coolant exiting the channel. It is important to avoid approximations in the evaluation of convection between tank and vessel external shell to investigate the eddies-generated local hotspots. Recirculating flows in peripheral regions are not an issue for thermal analysis due to the significantly lower volumetric heat deposition, despite their size may be larger than near-vessel eddies. Also, vacuum vessel channels have an evident impact on vacuum vessel external materials, leading to higher vessel temperatures as the fluid heats up. The combination of high channel temperatures, which occur towards channel outlets, and hotspots originating from near-vessel eddies in the tank will most likely raise criticalities. While the heat transfer coefficient increases in the channel region may improve the vessel cooling conditions,

different vessel geometries and inlet/outlet configurations should be explored to limit eddies generation.

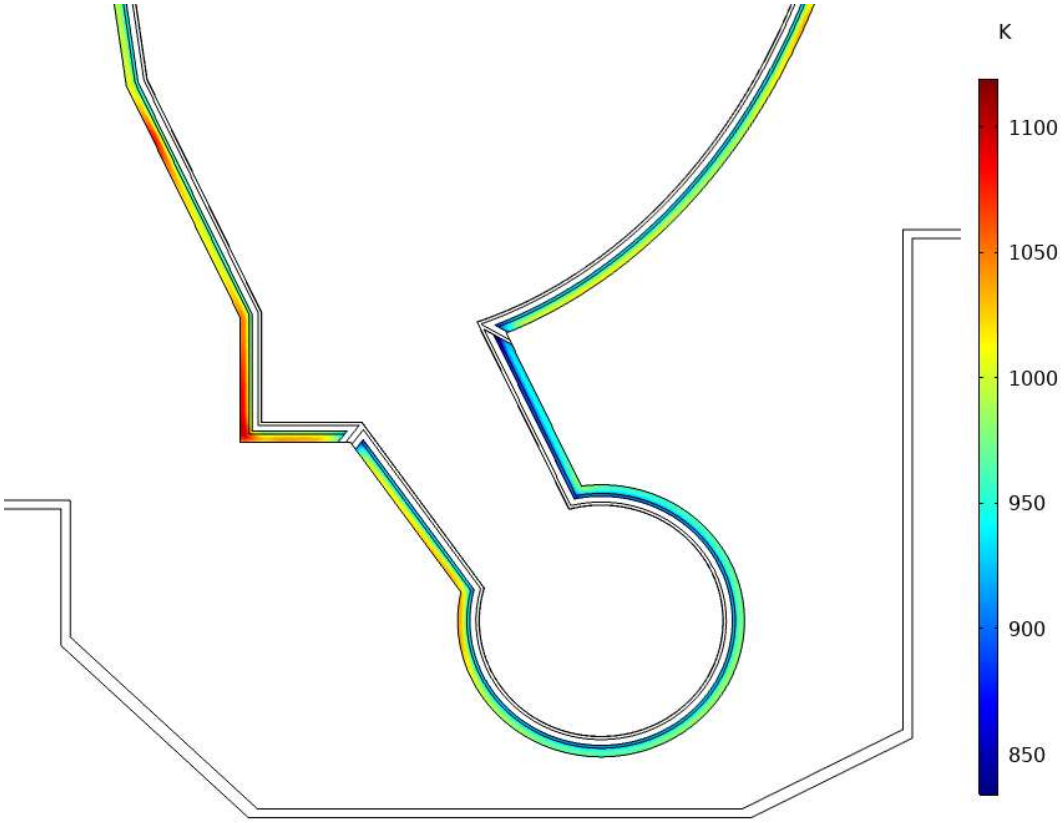

Figure 10 External vessel temperature and hotspots on the lower vessel region.

Blanket inlet and outlet configurations are slightly different from the initial hypothesis [1]. Simulations with the original configuration showed no cooling contribution from the auxiliary inlet. The FLiBe flow from the auxiliary inlet went directly towards the outlet, providing poor cooling to the tank. Results with the redesigned configuration show that FLiBe from the auxiliary tank inlet flows across the whole reactor, while a smaller fraction of FLiBe directed towards the outlet recirculates (Figure 11). Larger auxiliary inlet flowrates can help in cooling the blanket and prevent recirculation. However, outlet temperature would decrease as a consequence, lowering the plant thermodynamic efficiency. In this configuration, the outlet temperature is approximately 900 K and the average temperature is 892 K with an inlet temperature of 800 K. The average is much closer to outlet temperature due to recirculation across the blanket and localized hotspots.

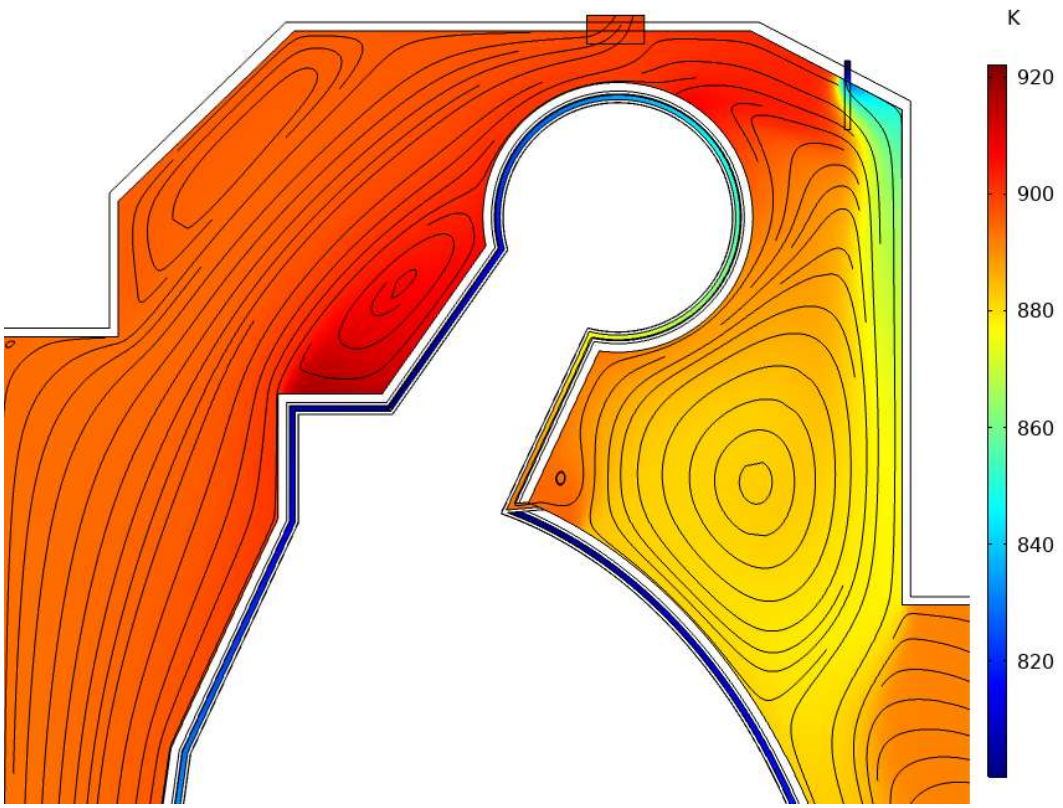

Figure 11 Tank temperature distribution near the upper divertor region, with a redesigned tank auxiliary inlet

IV.C Tritium transport

Tritium concentration in FLiBe is lower in channel regions, near the inlet, and increases in the tank region. Eddies increase tritium concentration, especially in high tritium generation areas near the vacuum vessel. The average tritium concentration in the tank is an order of magnitude higher than in the channels. Because of eddies and recirculation, the outlet tritium concentration is lower than the tank average concentration. The largest tritium concentration in FLiBe is found in a recirculating flow near the upper divertor region, towards the outboard (Figure 12).

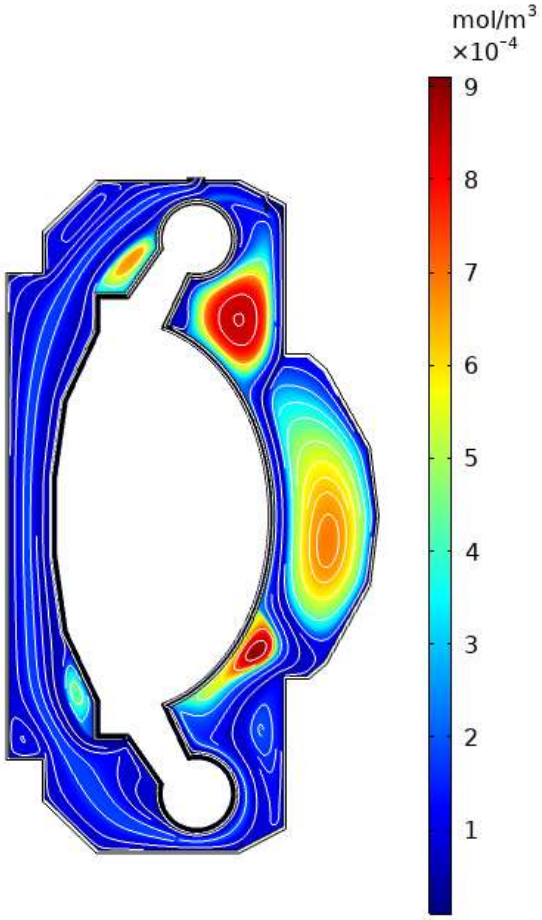

Figure 12 ARC Tritium concentration in FLiBe. The highest tritium concentration is found in recirculating areas.

Tritium concentration in vacuum vessel layers depends highly on transport properties of the material: while Tungsten and Beryllium average tritium concentrations are of the same order of magnitude as in FLiBe, tritium concentration in Inconel 718 is significantly higher (TABLE V) due to a higher Sievert's constant.

TABLE V Tritium concentrations and inventories in ARC VV and blanket

Domain	**Inventory $[g]$**	**Average Concentration $[mol/m^3]$**
FLiBe channel	$2.13 \cdot 10^{-3}$	$4.60 \cdot 10^{-5}$
FLiBe Tank	0.75	$4.04 \cdot 10^{-4}$
Inconel Vessel	1.33	$2.88 \cdot 10^{-2}$
Inconel tank shell	1.07	$2.30 \cdot 10^{-2}$
Tungsten	$1.34 \cdot 10^{-4}$	$1.17 \cdot 10^{-4}$
Beryllium	$6.91 \cdot 10^{-3}$	$6.03 \cdot 10^{-4}$

A total inventory of 3.16 g is found in ARC blanket. Inconel 718 tritium inventory is 76% of the total inventory, while the second-highest contribution (23.8%) comes from FLiBe.

V. Discussion

Results for the channel region show the importance of fractioning the vacuum vessel cooling in different segments to obtain a more uniform velocity distribution. The most susceptible segments to acceleration due to toroidal geometry are the divertor channels, due to higher radial excursion, but, being shorter than central vessel channels, it should be possible to lower the flowrate to satisfy the corrosion threshold without exceeding temperature limits for VV materials. Channel CFD analysis highlights that channel design should have particular attention on sharp turning points due to vena contracta accelerating the flow locally and the impact of axis distance on FLiBe flow section, therefore its velocity. Results show inadequate heat transfer coefficient in channel regions, leading to vacuum vessel overheating. The channel model does not describe the final design accurately due to 2D approximation, but provides a first modeling of tritium transport and channel flow. While increasing the velocity can enhance heat transfer, corrosion thresholds may not allow for it. If a corrosion control system is not employed, a heat transfer enhancement study by modifying the channel geometry must be carried out. For tank region, the recirculating flow across the blanket result in an increase in temperature and tritium concentration. Also, eddies are responsible for an increase in tritium concentration, both in FLiBe and in adjacent materials. This phenomenon is more evident near the vacuum vessel. Behind the high tritium solubility in Inconel 718, eddies are the second responsible for increased tritium inventory in ARC, both in FLiBe (which is relevant in case of accidental release) and in structural materials facing the external environment (important for routine permeation-driven leakage and maintenance).

VI. Conclusions

The work presented in this paper represents a first step to evaluate how FLiBe behaves inside the ARC blanket and estimate tritium inventory, which is crucial for ARC economy and safety. A CFD and tritium transport analysis has been carried out by means of COMSOL® Multiphysics. From the thermo-fluid-dynamic viewpoint, this preliminary study underlines the importance to model the FLiBe channel and the tank as a unique system to take into account the possible generated hotspots when evaluating vessel temperature distribution. A detailed channel simulation, which models carefully the tank boundary condition or includes the tank region in the model, is needed to evaluate vessel temperatures in a realistic design with suitable heat transfer coefficients. In addition, some considerations on the geometry have been derived from this work. The localization of an additional inlet with respect to the reference geometry has been investigated. As far as the tritium transport is concerned, this performed analysis highlights that the higher concentration of tritium is in the Inconel 718 (76%) and then in the FLiBe tank (23%), for a total tritium inventory of $3.16\ g$. An increase of Inconel 718 volume in further design development will probably result in a proportional increase in inventory. These results show that Inconel can act as a sink for tritium during transients in the first hours of operation, and therefore increase the start-up inventory. Moreover, the results highlight that the average tritium concentration in FLiBe can be greater than outlet concentrations and that the flow field in the tank region has a significant impact on tritium inventory in steady-state conditions. Therefore, a CFD analysis is necessary to not underestimate total tritium inventory. Obtained results can be employed as a starting point for transient simulation to evaluate tritium fluxes to obtain characteristic times, and leakage due to permeation through structural materials.

Future works will focus on the design of a reliable channel design with a suitable heat transfer coefficient, and the implementation of a MHD 3D model. Future works will also include an improvement of the tritium transport model by considering additional phenomena such as time-dependent behavior, and tritium speciation analysis.

References

[1] B. N. SORBOM *et al.*, "ARC: A Compact, High-field, Fusion Nuclear Science Facility and Demonstration Power Plant with Demountable Magnets," *Fusion Eng. Des.*, vol. 100, pp. 378–405, 2015.

[2] A. Q. KUANG *et al.*, "Conceptual Design Study for Heat Exhaust Management in the ARC Fusion Pilot Plant," *Fusion Eng. Des.*, vol. 137, no. August, pp. 221–242, 2018, doi: 10.1016/j.fusengdes.2018.09.007.

[3] M. R. K. WIGRAM *et al.*, "Performance Assessment of long-legged Tightly-baffled Divertor Geometries in the ARC Reactor Concept," *Nucl. fusion*, vol. 59, no. 10, p. 106052, 2019.

[4] M. ZUCCHETTI, Z. HARTWIG, S. MESCHINI, S. SEGANTIN, R. TESTONI, and D. WHYTE, "ARC Reactor: Radioactivity Safety Assessment and Preliminary Environmental Impact Study," *Fusion Eng. Des.*, vol. 162, p. 112132, 2021.

[5] S. MESCHINI, R. TESTONI, S. SEGANTIN, and M. ZUCCHETTI, "ARC Reactor: A Preliminary Tritium Environmental Impact Study," *Fusion Eng. Des.*, vol. 167, no. November 2020, p. 112340, 2021, doi: 10.1016/j.fusengdes.2021.112340.

[6] H. NAKAHARAI *et al.*, "The Influence of a Magnetic Field on Turbulent Heat transfer of a High Prandtl Number Fluid," *Exp. Therm. Fluid Sci.*, vol. 32, no. 1, pp. 23–28, 2007.

[7] B. R. MUNSON, T. H. OKIISHI, W. W. HUEBSCH, and A. P. ROTHMAYER, *Fluid mechanics*. Wiley Singapore, 2013.

[8] T.-H. SHIH, *A Realizable Reynolds Stress Algebraic Equation Model*, vol. 105993. National Aeronautics and Space Administration, 1993.

[9] A. Fluent, "12.0 User's Guide," *Ansys inc*, vol. 6, 2009.

[10] A. B. Comsol, "CFD Module User's Guide." Version, 2015.

[11] S. SEGANTIN, R. TESTONI, and M. ZUCCHETTI, “Neutronic Comparison of Liquid Breeders for ARC-like Reactor Blankets,” *Fusion Eng. Des.*, vol. 160, p. 112013, 2020.

[12] D. A. PETTI *et al.*, “JUPITER-II Molten salt Flibe Research: An Update on Tritium, Mobilization and Redox Chemistry Experiments,” *Fusion Eng. Des.*, vol. 81, no. 8–14, pp. 1439–1449, 2006.

[13] M. ABDOU *et al.*, “Physics and Technology Considerations for the Deuterium–Tritium fuel Cycle and Conditions for Tritium Fuel self Sufficiency,” *Nucl. fusion*, vol. 61, no. 1, p. 13001, 2020.

[14] A. PERUJO, K. DOUGLAS, and E. SERRA, “Low Pressure Tritium Interaction with Inconel 625 and AISI 316 L Stainless Steel Surfaces: an Evaluation of the Recombination and Adsorption Constants,” *Fusion Eng. Des.*, vol. 31, no. 2, pp. 101–108, 1996.

[15] P. HUMRICKHOUSE, “Tritium Transport, Permeation, and Control,” 2016, [Online]. Available: https://nucleus.iaea.org/sites/fusionportal/Technical Meeting Proceedings/4th DEMO/website/talks/November 15 Sessions/Humrickhouse.pdf.

[16] P. J. ROACHE, K. N. GHIA, and F. M. WHITE, “Editorial Policy Statement on the Control of Numerical Accuracy,” *J. Fluids Eng.*, vol. 108, no. 1, p. 2, Mar. 1986, doi: 10.1115/1.3242537.

[17] W. L. OBERKAMPF and C. J. ROY, *Verification and Validation in Scientific Computing*. Cambridge University Press, 2010.

[18] M. CASEY and T. WINTERGERSTE, “ERCOFTAC best Practice Guidelines for Industrial Computational Fluid Dynamics,” *Ercoftac, Brussels*, p. 82, 2000.

[19] D. OLANDER, “Redox Condition in Molten Fluoride Salts: Definition and Control,” *J. Nucl. Mater.*, vol. 300, no. 2–3, pp. 270–272, 2002.

[20] H. NAKAMURA *et al.*, “Case Study on Tritium Inventory in the Fusion DEMO Plant at JAERI,” *Fusion Eng. Des.*, vol. 81, no. 8–14, pp. 1339–1345, 2006.

[21] D. J. MITCHELL and E. M. EDGE, “Permeation Characteristics of some Iron and Nickel Based Alloys,” *J. Appl. Phys.*, vol. 57, no. 12, pp. 5226–5235, 1985.

[22] E. ABRAMOV, M. P. RIEHM, D. A. THOMPSON, and W. W. SMELTZER, “Deuterium

Permeation and Diffusion in High-purity Beryllium," *J. Nucl. Mater.*, vol. 175, no. 1–2, pp. 90–95, 1990.

[23] P. CALDERONI, P. SHARPE, M. HARA, and Y. OYA, "Measurement of Tritium Permeation in Flibe (2LiF–BeF2)," *Fusion Eng. Des.*, vol. 83, no. 7–9, pp. 1331–1334, 2008.

[24] M. UTILI *et al.*, "Tritium Extraction from hcll/wcll/dcll pbli bbs of Demo and hcll tbs of Iter," *IEEE Trans. Plasma Sci.*, vol. 47, no. 2, pp. 1464–1471, 2019.

[25] S. SEGANTIN, "Load Following Concept Feasibility of ARC Reactor Power Plant Based on the Thermo-mechanical Analysis of the Vacuum Vessel." Master thesis at Politecnico di Torino, 2017.

List of Figures and Tables

TABLE V Tritium concentrations and inventories in ARC VV and blanket